

Detection of three-dimensional crustal movements due to the 2011 Tohoku, Japan Earthquake from TerraSAR-X intensity images

W. Liu^{*a}, F. Yamazaki^b, T. Nonaka^c, T. Sasagawa^c

^{a, b} Dept. of Urban Environment Systems, Chiba Univ./ 1-33 Yayoi-chou, Inake-ku, Chiba, Japan, 263-8522; ^a JSPS research fellow

^c Satellite Business Division, PASCO/Meguro Building Annex, 2-8-10 Higashiyama, Meguro-ku, Tokyo, Japan, 153-0043

ABSTRACT

The Tohoku earthquake on March 11, 2011 caused widespread devastation and significant crustal movements. According to the GPS Earth Observation Network System (GEONET) operated by Geospatial System Institution (GSI) of Japan, crustal movements with a maximum of 5.3 m to the horizontal direction (southeast) and a maximum of 1.2 m to the vertical direction (down) were observed over wide areas in the Tohoku (north-western) region of Japan. A method for capturing the two-dimensional (2D) surface movements from pre- and post-event TerraSAR-X (TSX) intensity images has been proposed by the present authors in our previous research. However, it is impossible to detect the three-dimensional (3D) actual displacement from one pair of TSX images. Hence, two pairs of pre- and post-event TSX images taken in ascending and descending paths respectively were used to detect 3D crustal movements in this study. First, two sets of 2D movements were detected by the authors' method. The relationship between the 3D actual displacement and 2D converted movement in SAR images was derived according to the observation model of the TSX sensor. Then the 3D movements were calculated from two sets of detected movements in a short time interval. The method was tested on the TSX images covering the Sendai area. Comparing with the GEONET observation records, the proposed method was found to be able to detect the 3D crustal movement at a sub-pixel level.

Keywords: Crustal movement, the 2011 Tohoku earthquake, TerraSAR-X, three-dimensional displacement

1. INTRODUCTION

The Mw 9.0 Tohoku Earthquake occurred on March 11, 2011, off the Pacific coast of northeastern (Tohoku) Japan, caused gigantic tsunamis, resulting in widespread devastation. The epicenter was located at 38.322° N, 142.369° E at a depth of about 32 km. The earthquake resulted from a thrust fault on the subduction zone plate boundary between the Pacific and North American plates. According to the GPS Earth Observation Network System (GEONET) at the Geospatial Information Authority (GSI) in Japan, crustal movements with maximums of 5.3 m to the horizontal (southeast) and 1.2 m to the vertical (downward) directions were observed over a wide area [1]. Although GSI has established about 1,200 GPS ground control stations throughout Japan, the distance between two neighboring stations is over 20 km. Hence, it remains difficult to capture a detailed crustal movement distribution using only GPS recordings. It is also difficult for developing countries to establish GPS recording systems. Thus, estimating crustal movements from satellite data is considered to be an efficient and important method.

Two methods have normally been used to detect crustal movements from remote sensing images in the past studies. The first one is interferometric (InSAR) analysis of synthetic aperture radar (SAR) [2]. Several studies have been conducted to detect displacements due to earthquakes based on differential SAR interferometry (DInSAR) [3, 4]. However, depending on vegetation and temporal decorrelation [5], InSAR may not always be able to measure ubiquitous deformation at a large scale. In addition, InSAR analysis can only detect movements to the slant range direction. The second method is the pixel-offset method, which can be applied to both SAR and optical images. Michel *et al.* [6] and Tobita *e.al.* [7] measured ground displacements after earthquakes using SAR amplitude images. Crippen [8], Leprince *et al.* [9], and González *et al.* [10] also detected ground deformation in SPOT and IRS panchromatic imagery. Using the method, two images are co-registered for non-displaced boundaries, before internal local deformation is calculated by cross-correlation. The merit of the pixel-offset method is that it can detect the movement to two directions. Since the real

crustal movement is a three-dimensional (3D) vector, 3D surface displacement estimates have been obtained by both InSAR and pixel-offset methods using SAR image pairs captured from ascending and descending orbits [11-13].

In the 2011 Tohoku earthquake, the extent of crustal movements was much larger than the SAR imaging area. Due to the absence of the accurate geocoding information, it was difficult to detect the absolute displacement using the previous two methods. The high-accuracy georeferenced product, however, has become available recently due to the improvement of SAR sensors, and thus an improved pixel-offset method was proposed by the present authors to estimate the absolute ground displacements even in the case of large-scale tectonic movements [14]. In our previous research, the proposed method has been tested on four temporal TerraSAR-X (TSX) images along the Sendai coastal land with a 37.3° incident angle at the center, and high accuracy was obtained. The maximum error between the GPS observed data and the detected result was less than 0.5 m. Comparing with the 3.0 m spatial resolution of the StripMap mode TSX., the proposed method has the capability to detect crustal movement at a sub-pixel level.

In this study, two pairs of the pre- and post-event TSX intensity images from the Tohoku earthquake taken in ascending and descending paths respectively, were used to detect crustal movements by the propose method based on the shifts of non-changed buildings. Then the real 3D movement was calculated from the two set of detected results based on SAR intensity data. The accuracy of both 2D and 3D detection results was demonstrated, comparing the detected displacements with those from GPS ground station records.

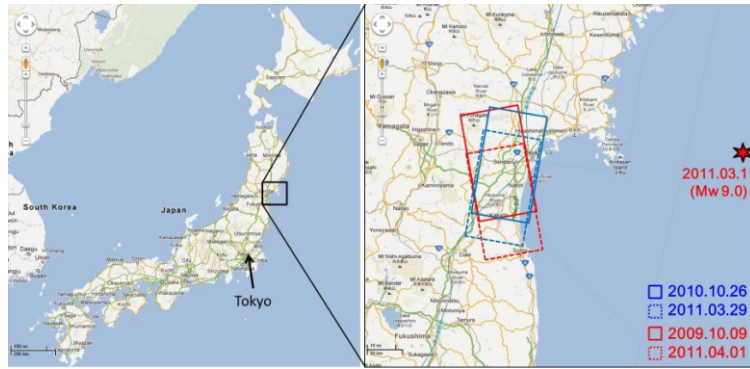
2. IMAGE DATA AND PREPROCESSING

The study area was focused on the coastal zone of Tohoku, Japan, as shown in Figure 1(a), which was one of the most severely affected areas in the 2011 Tohoku earthquake. Four temporal TSX images taken before and after the earthquake are shown in Figure 1(b-e), which we used for detecting crustal movements. In the ascending pair, the pre-event image was taken on October 9, 2009 (Local time), while the post-event ones were taken on April 1, 2011. There is a 35.23° incident angle at the center of the images. The heading angle is 349.79° clockwise from the north. In the descending pair, the pre-event image was taken on October 26, 2010, while the post-event ones were taken on March 29, 2011. There is a 21.47° incident angle at the center of the images. The heading angle is 19.32° clockwise from the north.

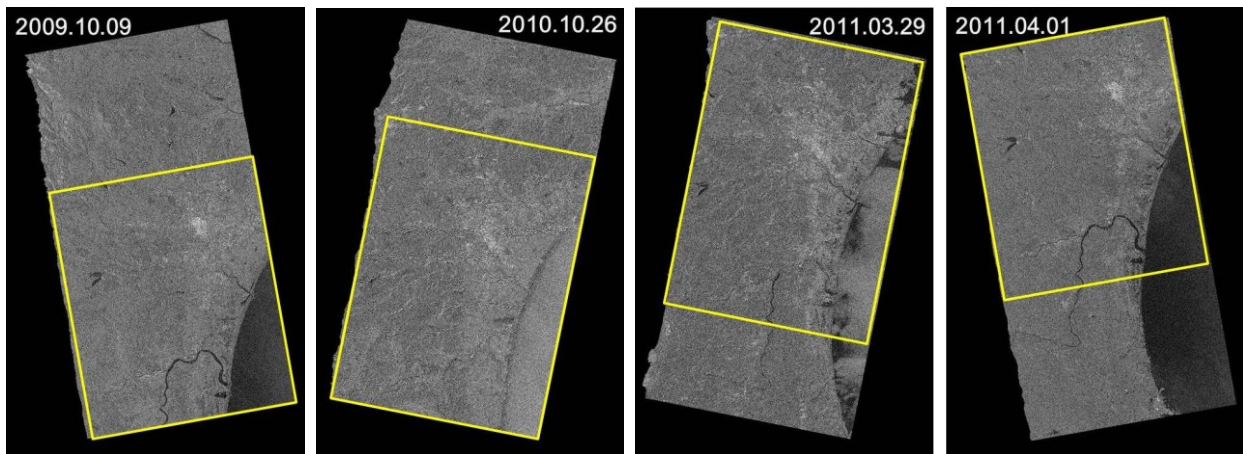
All these images were captured with HH polarization and in the StripMap mode. Due to the different incident angles, the resolutions of the ascending pair in the azimuth and range directions were both about 3.0 m, while those of the descending pair were 3.0 m in the azimuth and 3.5 m in the range directions. We used the standard Enhanced Ellipsoid Corrected (EEC) products as processing level 1B, where the image distortion caused by a variable terrain height was compensated using a globally available digital elevation model (SRTM). The products were provided in the form projected to a WGS 84 reference ellipsoid with a resampled square pixel size of 1.25 m.

Since the four images covered the different areas, the target area was set as the common part of the yellow frame in Figure 1(b-e). Two preprocessing approaches were applied to the images before extracting crustal movements. First, the four TSX images were transformed to a Sigma Naught (σ^0) value, which represents the radar reflectivity per unit area in the ground range. Then an Enhanced Lee filter was then applied to the original SAR images to reduce the speckle noise. Since the speckle noise reduces the correlation between two TSX images, applying an adaptive filter can improve the accuracy of the detection. To minimize any loss of information included in the intensity images, the window size of the filter was set as 3×3 pixels. The pixel localization corrected by the GPS orbit determination was used directly in this study, and thus the accuracy of the proposed method depends on the accuracy of the products. According to the product specification document [15], the pixel localization accuracy of the EEC products depends on the orbit and the DEM used. Since the four EEC products were made using the same DEM following the same process, the errors caused by the DEM were cancelled out when comparing two images [16]. Thus the major cause of error here comes from the orbit accuracy. Since the orbit type of our TSX images was "Science", their required orbit accuracy is within 20 cm, but actual data showed better than 10 cm accuracy [17].

After the preprocessing approach, two color composites images of the ascending and descending pairs were shown in Figure 2(a-b), where the pre-event image was assigned as green and blue bands while the post-event image as red band. The ascending pair covers five GPS ground stations, which named Rifu, Sendai, Miyagi-kawasaki, Natori and Watari from the north to the south. The descending pair covers four stations except Miyagi-kawasaki. A close-up of the descending pair near Sendai station is shown in Figure 2(c). From the stretched TSX intensity images, the displacements



(a)



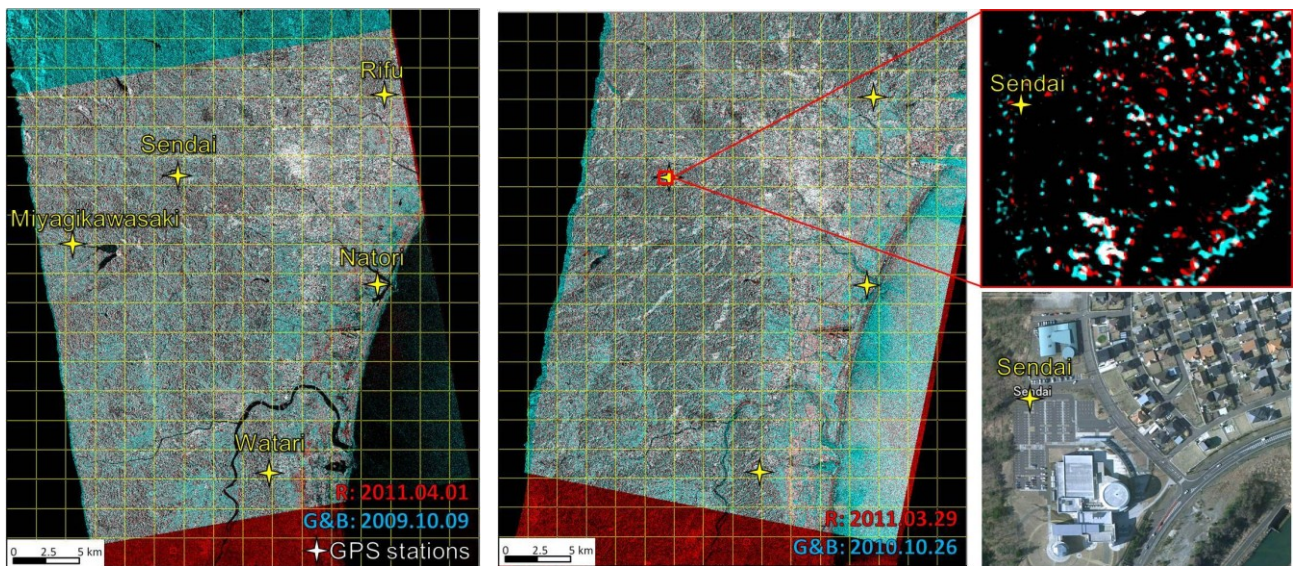
(b)

(c)

(d)

(e)

Figure 1. Study area along the Pacific coast of Tohoku, Japan (a); the pre-event TSX image taken on October 9, 2009 (b) and October 26, 2010 (c); the post-event images taken on March 29 (d) and April 1, 2011 (local time) (e).



(a)

(b)

(c)

Figure 2. Color composite images of the ascending (a) and descending (b) pairs; close-up of (b) around Sendai GPS station and its optical image taken on April 6, 2011, cited from Google Earth (c)

of a white building in bottom left of the optical image, which is shown in the bottom of Figure 2(c), can be seen in different colors. The building is an observatory which was not damaged during the earthquake. Thus, the displacement between the two TSX images is considered due to the crustal movement.

3. TWO-DIMENSIONAL DETECTION

GSI has established about 1,200 GPS-based control stations throughout Japan. The movement of the land of Japan is daily monitored by GEONET's GPS. The observation data from the network are available for actual survey works and for the studies of earthquakes and volcanic activities. In this earthquake, the movements about 5.3 m horizontally and 1.2 m vertically were observed after the main shock. Several small changes were continuously observed also in the subsequent aftershocks. The vector images of the observed variation at the GPS control stations during the period of March 11 to 13, 2011 to the horizontal and vertical directions are shown in Figure 3(a-b). The largest displacement occurred along the coastline of Tohoku region, and displacements were observed in more than half of the country. The target area was shown by red frame in Figure 3(a-b) where significant movements are seen at all the five GPS stations.

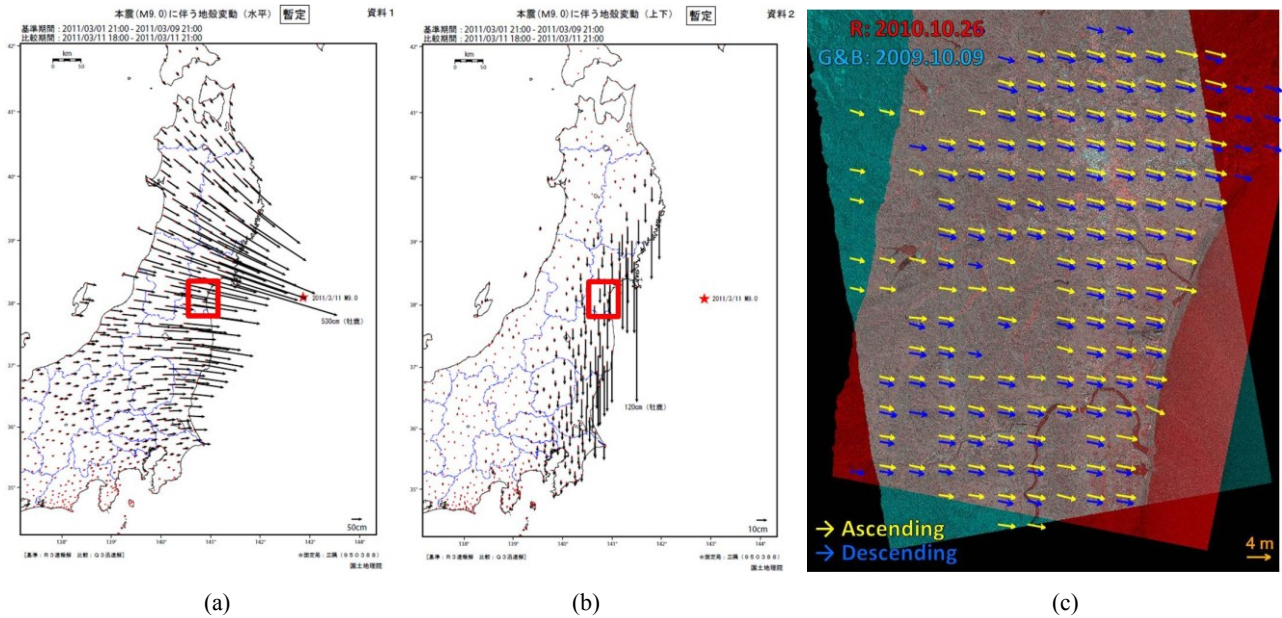
The crustal movements within the target area were extracted by the proposed pixel-offset method [14]. Firstly, the whole target area was divided into a $2.5 \times 2.5 \text{ km}^2$ mesh, as shown in Figure 2(a-b). In each sub-area ($2.5 \times 2.5 \text{ km}^2$), solid buildings larger than 150 m^2 were extracted by a simple segmentation approach. The threshold value of the backscattering intensity used in segmentation was set as -2.5 dB, which means the pixels of larger than -2.5 dB were grouped as a building object. Then the non-changed buildings were extracted by comparing the building locations in the two building images. If a solid building exists in the post-event image around the location of a target building in the pre-event image within 5 pixels, the target building is regarded as non-changed. The displacement of a non-changed building between the two TSX intensity images was calculated by an area correlation method. To improve the accuracy, the TSX images surrounding non-changed structures were resampled to 0.25 m/pixel by cubic convolution to have 1/5 of the original pixel size. Thus, the shift of building shapes could be detected at a sub-pixel level.

A target area was selected from the pre-event intensity image at the location of a non-changed building object. Then a search area, which surrounds the target area and exceeds it in size, was selected in the post-event intensity image. The target area was overlaid with the search area and was shifted within it. In each shift, a similarity index was calculated. The similarity matrix contained the values of the statistical comparison between the target and search areas. The maximum value in the matrix was determined as the correlation coefficient of the building, and the location of the maximum value was considered as the final offset of the target in the search area. When the correlation coefficient of a non-changed building in the two TSX image was larger than 0.8, the detected displacement was counted as valid data. The crustal movements in the whole area were detected in the same way. Finally, the average value of these movements was calculated and considered as the crustal movement in that sub-area. To ensure the reliability of the results, only a sub-area containing more than 5 building displacements was counted as valid one.

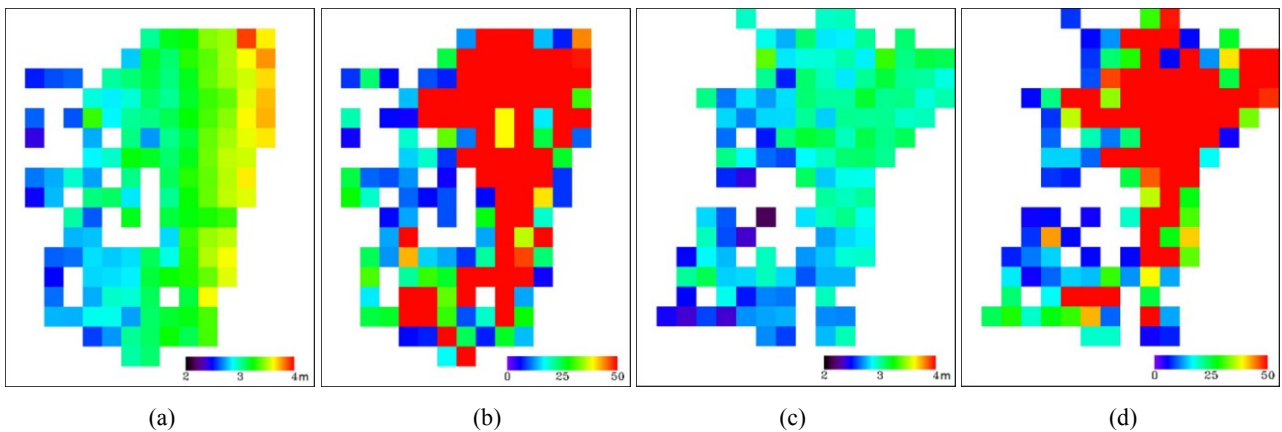
3.1 Ascending pair

The authors' method was applied on the ascending pair of TSX intensity images. Since the displacements were calculated from the location of buildings, the proposed method could not be applied to mountainous areas without buildings. The movements from 145 sub-areas (about 900 km^2) were detected, and they are shown in Figure 3(c) by the yellow vectors. The average value of the detected movements was 3.00 m to east and 0.68 m to south. The displacements of five sub-areas including the GPS stations were all detected, and their values were shown in Table 1. A comparison of the detected movements in the table shows that the largest movement occurred around Rifu GPS station, which is the nearest one from the epicenter.

The displacement amplitude is shown in Figure 4(a) by a rainbow color. The largest detected movement was 3.87 m with 3.75 m to the east and 0.89 to the south directions. The number of displacements detected in each sub-area is shown in Figure 4(b). The more number of the detected displacements were, the more reliable the result became. The detect result became stable when the number of detected displacements were more than 10. Thus, our method shows higher accuracy in urban areas than in rural areas..



(a) (b) (c)
 Figure 3. GPS observed displacement vector in the period of March 11 to 13, 2011 in the horizontal (a) and vertical directions (b), cited from the GSI website; the detected displacement vectors in each sub-area overlapping on the color composite of the pre-event TSX images (c);



(a) (b) (c) (d)
 Figure 4. Displacement amplitude shown in rainbow color from the ascending (a) and descending pairs (c); and the number of buildings used in each sub-area from the ascending (b) and descending (d) pairs.

3.2 Descending pair

The method was also applied to the descending pair to detect the 2D movements. The displacements were detected from 130 sub-areas (about 800 km²), and they are shown in Figure 3(c) by blue vectors. The average value of the detected movements was 2.75 m to the east and 0.64 m to the south. The displacement amplitude is shown in Figure 4(c) by a rainbow color, while the number of displacements in each sub-area is shown in Figure 4(d). The largest detected movement from the descending pair was 3.35 m with 3.22 m to the east and 0.90 m to the south directions. The displacements of four sub-areas including GPS stations except Miyagi-wakasaki were all detected, and their values were also shown in Table 1.

Comparing with the results from the ascending pair, the detected movements from the descending pair were seen to be smaller. Since the time lag between the post-event images in the ascending and descending paths was only two days, the crustal movements can be considered almost the same level. The difference between the two results was caused by the

different incident angle and observation directions. But, the detected vectors in the both results were seen to line up to the similar directions..

4. THREE-DIMENSIONAL ESTIMATION

The surface displacement is a vector in the three-dimensional space with three components, D_E , D_N , and D_Z , to the east, north, and vertical directions, respectively. The relationship between an actual 3D crustal movement and its 2D version in a SAR image is shown in Figure 5(a-b). The proposed pixel-offset method can detect a 2D movement, in which the 3D movement is transformed to the east and north directions. The movement to the vertical direction is decomposed and transformed to the movements to the east and north directions. The relationship between an actual 3D crustal movement and its 2D shift in a ground range SAR image is shown in Equation (1).

$$\begin{pmatrix} M_E \\ M_N \end{pmatrix} = \begin{pmatrix} 1 & 0 & -\cos \alpha / \tan \theta \\ 0 & 1 & \sin \alpha / \tan \theta \end{pmatrix} \begin{pmatrix} D_E \\ D_N \\ D_Z \end{pmatrix} \quad (1)$$

where D is the actual movement to the east, north, and vertical directions; M is the shift in the SAR image; α is the heading angle clockwise from the north; and θ is the SAR incident angle.

From one pair of the TSX images, the detected 2D result is not enough to estimate the 3D movement. However, two pairs of different observation sets can build four individual equations, and it makes the 3D estimation possible. If the crustal movements included in the two pairs of TSX images are the same, then the vertical movements can be calculated either from Equation (2) or Equation (3).

$$D_{Z1} = \frac{M_{EAs} - M_{EDs}}{\cos \alpha_{Ds} / \tan \theta_{Ds} - \cos \alpha_{As} / \tan \theta_{As}} \quad (2)$$

$$D_{Z2} = \frac{M_{NAs} - M_{NDs}}{\sin \alpha_{As} / \tan \theta_{As} - \sin \alpha_{Ds} / \tan \theta_{Ds}} \quad (3)$$

where As and Ds represent the parameters in the ascending and descending paths respectively.

In theory, the obtained D_{Z1} using the results in the east direction and D_{Z2} using the results in the north direction are the same value. However, the vertical movements calculated by Equation (2) and (3) were somewhat different in this study, due to the two day time lag between the two pairs of data and the errors included in the detected results. From the D_{Z1} , one result in the east and two results in the north directions are obtained. Similarly from the D_{Z2} , two results in the east and one result in the north directions are obtained. Thus many possible combination of the 3D results exist.

In this study, four combinations were proposed and compared with the GPS records at the four GPS stations. The first set is using D_{Z1} directly as the vertical movement and then D_E and D_N were calculated from D_{Z1} and D_{Z2} , respectively. In this case, the results were all direct values without averaging. The second set is also using D_{Z1} directly as the vertical movement, and then one D_E was obtained and the average of different D_{Ns} were calculated using the D_{Z1} . The third set is using the average value of D_{Z1} and D_{Z2} as the vertical movement, while D_E and D_N were still calculated from different D_Z , respectively. The last set is using the average value of D_{Z1} and D_{Z2} as the vertical movement, and the average values of two different D_{Es} and D_{Ns} were used, which were calculated by the vertical value. In this cause, the movements in the three-dimensional space were all averaged values.

The 3D movements in the four sub-areas including GPS stations were calculated by the proposed combinations. Then their results were compared with the observed GPS data, and the Root Mean Square (RMS) error was calculated for each case. The result from the second set showed the lowest difference with the GPS data, and its RMS error was 0.20 m in the 3D space. Since a most part of the vertical movement was decomposed to the east direction than the north direction due to the parameters of the observation model, the D_{Z1} calculated from the results in the east direction was more stable than the one from the north direction.

Thus, the second combination was used to estimate the 3D movements in the whole target area. The detected result is shown in Figure 6(a). The yellow vectors were the movements in the horizontal and the blue ones were in the vertical

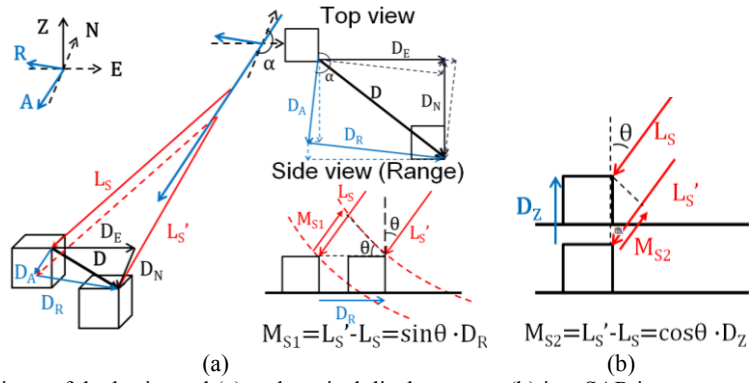


Figure 5. Schematic views of the horizontal (a) and vertical displacements (b) in a SAR image.

Table 1. Comparison of detected crustal movements in five sub-areas surrounding the GPS stations by the proposed method and the GPS records, to the 2D and 3D detections (unit: meter).

GPS station/ Component	Rifu			Sendai			Miyagi-kawasaki*			Natori*			Watari			
	E	N	Z	E	N	Z	E	N	Z	E	N	Z	E	N	Z	
2D As.	GPS	3.73	-0.87	—	2.97	-0.65	—	2.77	-0.49	—	3.66	-0.72	—	3.26	-0.62	—
	TSX	3.44	-0.95	—	2.74	-0.69	—	2.46	-0.59	—	3.47	-0.66	—	3.08	-0.54	—
	Error	-0.30	-0.082	—	-0.23	-0.04	—	-0.31	-0.10	—	-0.19	0.07	—	-0.18	0.08	—
2D Ds.	GPS	2.64	-0.71	—	2.41	-0.54	—	2.15	-0.43	—	2.79	-0.65	—	2.42	-0.43	—
	TSX	3.21	-0.69	—	2.58	-0.58	—	—	—	—	2.69	-0.38	—	2.67	-0.67	—
	Error	0.57	0.03	—	0.17	-0.04	—	—	—	—	-0.10	0.28	—	0.25	-0.24	—
3D	GPS	3.34	-0.86	-0.28	2.77	-0.61	-0.14	2.56	-0.52	-0.16	3.36	-0.77	-0.22	2.96	-0.54	-0.21
	TSX	3.36	-0.84	-0.06	2.68	-0.65	-0.04	—	—	—	3.19	-0.59	-0.20	2.93	-0.64	-0.11
	Error	0.02	0.02	0.22	-0.08	-0.04	0.10	—	—	—	-0.17	0.18	0.02	0.03	-0.10	0.10

* indicates the first GPS record after the observation resumed.

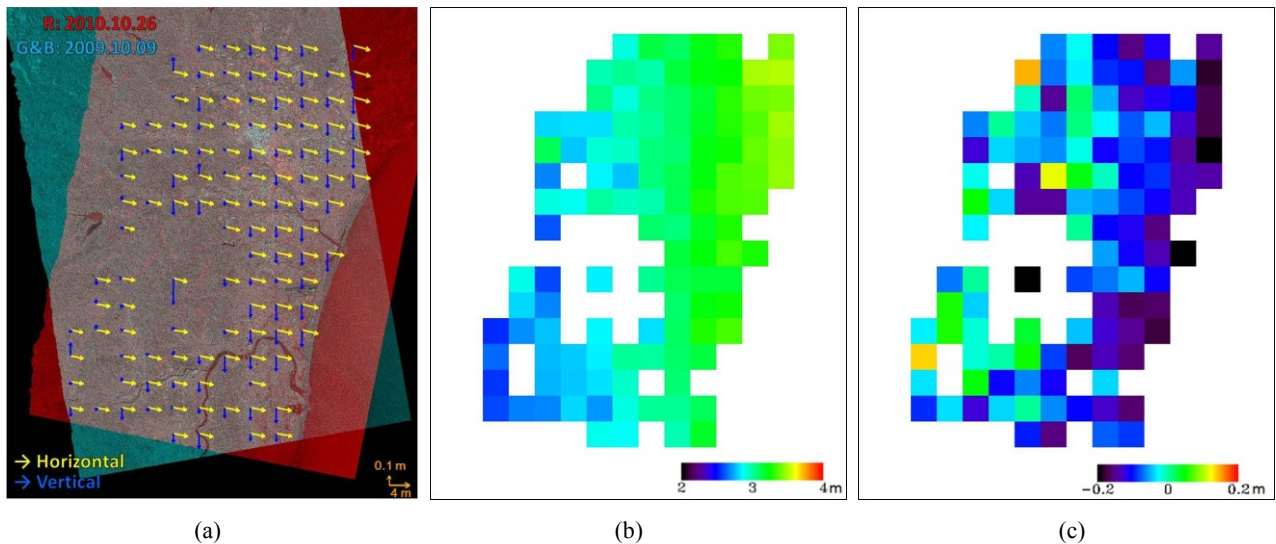


Figure 6. Detected 3D displacement vectors in each sub-area overlapping on the color composite of the pre-event TSX intensity images (a); the displacement amplitude in horizontal (b) and vertical (c) directions shown in rainbow color.

directions. Since the vertical movements were much smaller than the horizontal ones, they were shown in different scales. The displacement amplitude in the horizontal and vertical directions are shown in Figure 6(b) and (c), respectively by a rainbow color.

The 3D movements were detected for 116 sub-areas. The horizontal movements were in the range from 2.66 m to 3.38 m while the vertical ones were from -0.27 m to 0.14 m. From Figure 6(b), it can be confirmed that the largest movement occurred around the northeastern coast and the values were getting smaller as going southwards. The detected movement points to the east direction as the location goes to the south. This trend matched with the observed GPS data. The maximum subsidence was also occurred along the coast, and they were getting smaller as going westwards. These trends are also coincident with the observed GPS data shown in Figure 3(b). However, the detected results became unstable as going inside of the land. Several vertical results were seen to be different from those of the surrounding sub-areas..

5. VERIFICATION OF THE DETECTED RESULTS

To verify the accuracy of the detected 2D and 3D movements, the crustal movement data from the GPS stations were introduced. The GPS recordings obtained at Rifu, Sendai, Natori and Watari stations from March 1 to April 30, 2011 are shown in Figure 7. As the stations were located closer to the source region, more significant crustal movements were seen by the 2011 Tohoku Earthquake. Watari, Natori and Miyagi-kawasaki GPS stations stopped after the earthquake due to power outage and/or strong shaking. Natori GPS station was hit by tsunami waves and damaged and thus it did not restart until April 18, 2011. Miyagi-kawasaki station restarted after one month, on April 11, 2011. The estimation of crustal movements from SAR images provides important and effective information, especially in such cases.

A comparison of the 2D results detected around the five GPS stations with the converted GPS by Equation (1), is shown in Table 1. Since Natori and Miyagi-kawasaki stations did not restart until the middle of April, the displacements were calculated by the first record after restart. The detected results show a very high level of consistency with the GPS recordings. Based on the 9 comparison points, the averaged differences between our result and the GPS measurement were about 0.26 m to the east and 0.10 m to the north directions, respectively. The maximum differences were 0.57 m to the east (Rifu) and 0.28 m to the north (Natori) directions, as shown in Table 1. Both results were detected from the descending pair. It is considered that the accuracy of our method depends on the resolution of the TSX images. Since the range resolution for the descending pair was 3.5 m, larger than 3.0 m resolution for the ascending pair, the accuracy of the detected results is inferior for the case. In addition, the numbers of detected displacements around these two stations were both less than 15, which also caused the instability of the results. For these cases, changing the parameters in the segmentation approach can increase the number of displacements within a sub-area. However, it will take much more calculation time.

The comparison of the 3D results detected around the four GPS stations except Miyagi-kawasaki is also shown in Table 1. The average differences between our result and the GPS measurement were about 0.02 m in the horizontal and 0.11 m in the vertical directions. The maximum differences were 0.25 m in the horizontal (Natori) and 0.22 m in the vertical (Rifu), shown in Table 1. Since the vertical movement was calculated from the result in the east direction, large error around Rifu station in the descending path caused the error in the vertical direction. Thus, the accuracy of 3D movement estimation depends on the accuracy of the 2D movement detection. Our method, however, still showed high accuracy in both the 2D and 3D movement detection cases at a sub-pixel level.

6. CONCLUSIONS

In this study, we applied an enhanced pixel-offset method for detecting crustal movements due to a major earthquake on the basis of comparison between two temporal SAR intensity images. The method was tested using four temporal TerraSAR-X images covering the coast of Miyagi Prefecture, Japan before and after the 2011 Tohoku earthquake, which is a very difficult case as the geodetic displacement exceeded the SAR imaging area. The two-dimensional (2D) movements were detected both from the ascending and descending path pairs, and the three-dimensional (3D) movements were estimated according to these results. The four sub-areas surrounding GPS ground stations exhibited stable shifts of non-changed buildings and they were very similar to the observed GPS data. Subpixel-based matching made it possible to detect crustal movements with high accuracy, within 0.6 m in the 2D detection and 0.3 m in the 3D

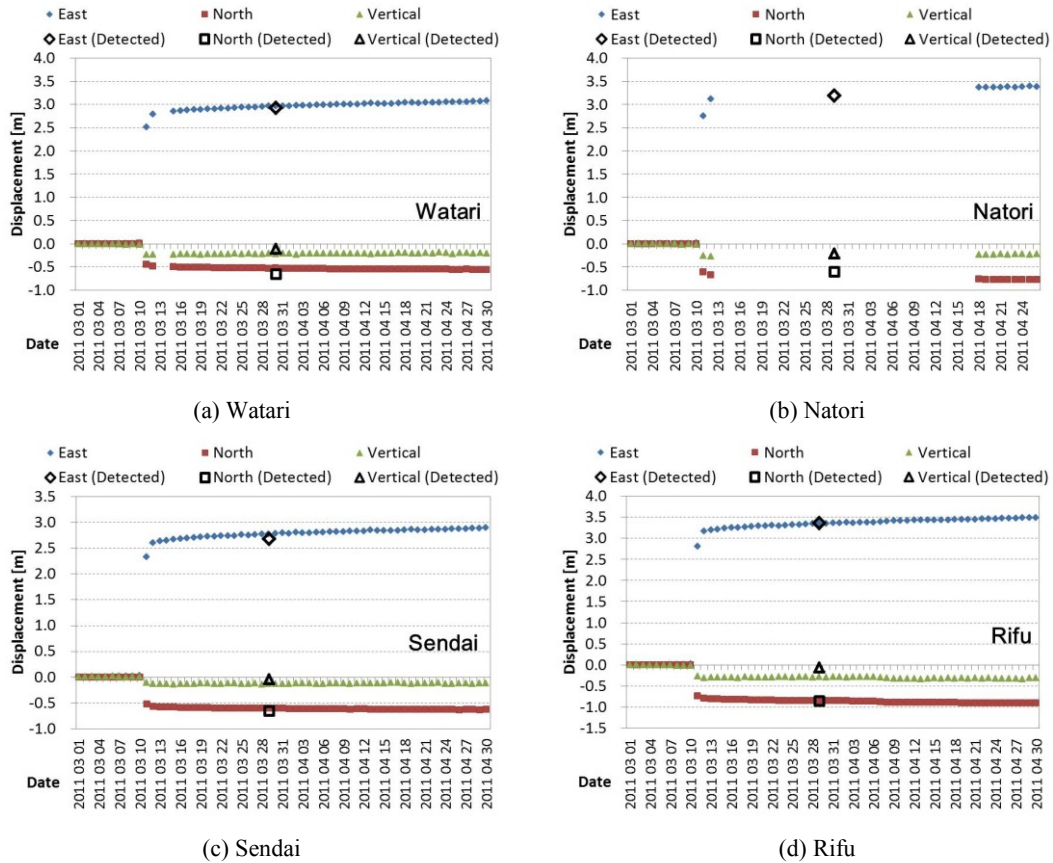


Figure 7. Comparison of movements converted from GPS data at Watari (a), Natori (b), Sendai (c), Rifu (d) ground control stations and the 3D results detected in surrounding sub-areas.

detection. We estimated 3D movements using the result in a sub-area unit ($2.5 \times 2.5 \text{ km}^2$) in this study, but the accuracy will be improved by estimating the 3D displacement for each building then taking their average for a sub-area. The accuracy of our method basically depends on the location accuracy of the original SAR images and the number of non-changed buildings. Although the results obtained in this study are promising, we will further test the proposed method for other events including smaller surface displacements to validate its applicability.

REFERENCES

- [1] Geospatial information Authority of Japan. Available: http://www.gsi.go.jp/BOUSAI/h23_tohoku.html#namelink3.
- [2] Zebker, H.A., "Studying the Earth with interferometric radar," *IEEE Computing in Science & Engineering*, 2(3), 52-60(2000).
- [3] Stramondo, S., Cinti, F. R., Dragoni, M., Salvi, S., and Santini, S., "The August 17, 1999 Izmit, Turkey, earthquake: Slip distribution from dislocation modeling of DInSAR and surface offset," *Annals of Geophysics*, 45(3/4), 527-536(2002).
- [4] Chini, M., Atzori, S., Trasatti, E., Bignami, C., Kyriakopoulos, C., Tolomei, C. and Stramondo, S., "The May 12, 2008, (Mw 7.9) Sichuan Earthquake (China): Multiframe ALOS-PALSAR DInSAR Analysis of Coseismic Deformation", *IEEE Geoscience and Remote Sensing Letters*, 7(2), 266-270(2010).
- [5] Bürgmann, R., Rosen, P.A., and Fielding, E.J., "Synthetic Aperture Radar interferometry to measure earth's surface topography and its deformation," *Annual Reviews Earth and Planet Sciences*, 28, 169-209(2000).
- [6] Michel, R., Avouac, J.-P., and Taboury, J., "Measuring ground displacements from SAR amplitude image: application to the Landers earthquake," *IEEE Geophysical Research Letters*, 26(27), 875-878(1999).
- [7] Tobita, M., Suito, H., Imakiire, T., Kato, M., Fujiwara, S., and Murakami, M., "Outline of vertical displacement of the 2004 and 2005 Sumatra earthquakes revealed by satellite radar imagery," *Earth Planets Space*, 48(1), e1-e4 (2006).
- [8] Crippen, R. E., "Measurement of sub resolution terrain displacements using SPOT panchromatic imagery," *International Journal of Remote Sensing*, 15(1), 56-61(1992).

- [9] Leprince, S., Barbot, S., Ayoub, F., and Avouac, J.-P., "Automatic and precise orthorectification, coregistration, and subpixel correlation of satellite images, Application to ground deformation measurements," *IEEE Trans. on Geos. Remote Sensing*, 45(6), 1529-1558(2007).
- [10] González, P. J., Chini, M., Stramondo, S., and Fernández, J., "Coseismic horizontal offsets and fault-trace mapping using phase correlation of IRS satellite images: The 1999 Izmit (Turkey) Earthquake," *IEEE Trans. on Geos. Remote Sensing*, 48(5), 2242-2250 (2010).
- [11] Fialko, Y., Simons, M., and Agnew, D., "The complete (3-D) surface displacement field in the epicentral area of the 1999 Mw7.1 Hector Mine earthquake, California, from space geodetic observations," *Geophysical Research Letters*, 28(16), 3063-3066(2001).
- [12] Catalão, J., Nico, G., Hanssen, R., and Catita, C., "Merging GPS and atmospherically corrected InSAR data to map 3-D terrain displacement velocity," *IEEE Trans. on Geos. Remote Sensing*, 49(6), 2354-2360(2011).
- [13] Michele, M. de, Raucoules, D., Sigoyer, J. de, and Pubellier, M., "Three dimensional surface displacement of the 2008 May 12 Sichuan earthquake (China) derived from Synthetic Aperture Radar: evidence for rupture on a blind thrust," *Geophysical Journal International*, 2010.
- [14] Liu, W., and Yamazaki, F., "2012. Detection of crustal movement from TerraSAR-X intensity image," *IEEE Geoscience and Remote sensing Letters*, DOI: 10.1109/LGRS.2012.2199076.
- [15] Eineder, M., Fritz, T., Mittermayer, J., Roth, A., Borner, E., Breit H., and Brautigam, B., "TerraSAR-X Ground Segment Basic Product Specification Document," TX-GS-DD-3302, Issue 1.7, 31-32(2010).
- [16] Breit, H., Fritz, T., Balss, U., Lachaise, M., Niedermeier, A., and Vonavka, M., "TerraSAR-X SAR processing and products," *IEEE Trans. on Geos. Remote Sensing*, 48(2), 727-739(2010).
- [17] Wermuth, M., Hauschild, A., Montenbruck, O., and Jäggi, A., "TerraSAR-X Rapid and Precise Orbit Determination," *21st International Symposium on Space Flight Dynamics*, France, 2009.